Displacement Damage in CMOS Image Sensors after Thermal Neutron Irradiation

Fabricio Alcalde Bessia, Martín Pérez, Miguel Sofo Haro, Iván Sidelnik, J. Jerónimo Blostein, Sergio Suárez, Pablo Pérez, Mariano Gómez Berisso and Jose Lipovetzky, *Member, IEEE*

***Abstract*—In this work CMOS image sensors were exposed to thermal neutrons observing an increase in the dark signal of many pixels. The effect was found to be similar to the damage caused by alpha particles irradiation. Rutherford backscattering spectroscopy and SIMNRA simulation were used to confirm that the sensors contain Boron in the insulation layers. The damage produced by thermal neutrons is explained as displacement damage caused by alpha particles and Lithium-7 ions in the Silicon active volume of the sensors after Boron-10 thermal neutron capture.**

***Index Terms*—Active pixel sensors, Alpha particles, CMOS image sensors, CMOS technology, Ionizing radiation, X-rays, Neutron radiation effects, BPSG, BoroPhosphoSilicate Glass, Thermal Neutron**

I. Introduction

In the past years much effort has been done on the detection of ionizing particles using CMOS image sensors [1]–[5]. It was also shown that Commercial Off the Shelf (COTS) CMOS active pixel sensors can be used for this purpose [2], [6]–[10] Particularly, [8], [9] deal specifically with the ability of this type of sensors to detect and count charged particles, gamma photons and X-rays, and the ability to distinguish between alpha particles and electrons or photons. Those articles focus on the possibility of using this kind of sensors as radiation dosimeters.

On the other hand, there has been an increased interest on the use of these devices as neutron detectors using special conversion layers, either over CMOS, CCD, or photodiodes for the detection of thermal neutrons [5], [11]–[14]. In general, conversion layers like ^{10}B, upon the interaction with thermal neutrons, release charged particles which are detected by the sensor. Recently, Gd was proposed as a conversion material on CMOS image sensors for high efficiency neutron detectors [14], [15].

In a previous work [16], a comparison of the effects of gamma photons, thermal neutrons and alpha particles on commercial of the shelf (COTS) CMOS image sensors has been made. The differences and similarities of the effect of those three types of ionizing radiation in CMOS image sensors were studied in a qualitative way. In this work we present a more detailed study concluding that thermal neutrons are captured by ^{10}B contained in the BoroPhosphoSilicate-Glass (BPSG) layers, which emits alpha particles and ^{7}Li ions, and which in turn produce displacement damage in the Silicon active volume of the sensor. To show this, a detection algorithm was developed to correlate damaged pixels with the ionization events. Then, the composition of the insulating layers was analyzed using the Rutherford Backscattering Spectroscopy technique, proving that they include ^{10}B in the BoroPhosphoSilicate-Glass (BPSG) layers. The results were explained and modeled through SRIM [17] simulations.

A similar mechanism—alpha or ^{7}Li emission after neutron trapping in BPSG—was repeatedly reported as a source for the generation of Single Event Upsets (SEUs) in logic cells and memories or soft errors in digital processors during thermal neutrons irradiation. For example *Baumann et. al.* demonstrated in [18] and [19] that the main cause of this effects was the interaction of environmental thermal neutrons with the BPSG layer used in fabrication processes. BPSG is typically used as interlevel and intralevel dielectric in several technology nodes. The addition of Boron to PSG reduces the reflow temperature and improves the fabrication process. Natural Boron contains about 20% of ^{10}B, which absorbs thermal neutrons and release charged particles that are the cause of SEUs in digital circuits. This undesired effect was used in [20] and [21] to develop a special thermal neutron detector. In those articles the BPSG layer was enriched with ^{10}B in order to increase the SEU or soft error rate of memory devices when exposed to thermal neutrons and then correlate the results to the incoming thermal neutron flux.

On the other hand, displacement damage caused by high energy neutrons has been reported several times. In [22] and [23] image sensors have been studied by *Theuwissen* over long time periods and reported that, although they were stored on shelf, there was an increase in leakage in some pixels which are seen as bright or *hot pixels* in the image. He related the generation of hot pixels to environmental high energy neutrons produced by cosmic rays. On the same line, [24] studied the generation of permanent errors—hot pixels—in image sensors. The SEU to permanent faults ratio has been calculated for three types of image sensors arriving to the conclusion that they were more sensitive than memory integrated circuits and that the hot pixels were generated also by cosmic rays. Fast neutrons cause displacement damage directly by impact against Si atoms. Displacement damage in CMOS image sensors was also reported several times [25],

Fabricio Alcalde Bessia <falcalde@ib.edu.ar>, José Lipovetzky <jose.lipovetzky@ieee.org>, Iván Sidelnik, Miguel Sofo Haro, J. Jerónimo Blostein, Mariano Gómez Berisso, and Sergio Suárez are with Balseiro Institute and CONICET. José Lipovetzky and Sergio Suárez are also with CNEA. Pablo Pérez is with CONICET. Martín Pérez <mperez@ib.edu.ar> is with CNEA. Jose Lipovetzky is also with ICTP.

This work was supported by ANPCyT under projects PICT 2014-1966 and PICT-2015-1644, UNCuyo C018, and by CONICET under projects PIP 2011-0552 and PIP 2013-0077.

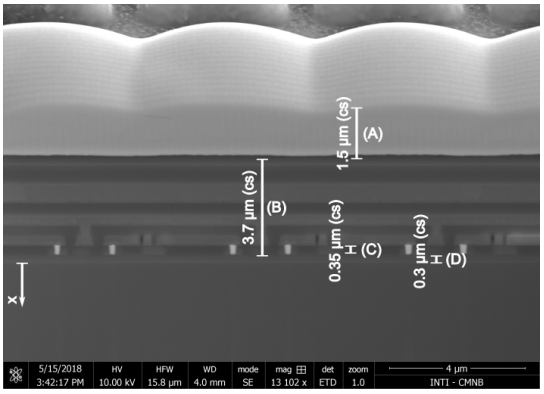

Fig. 1. SEM image of the cross-section of the integrated circuit. (A) Micro-lenses. (B) Back-End of Line. (C) Pre-Metal dielectric. (D) Field Oxide.

[26].

This work presents the displacement damage in CMOS image sensors as a result of thermal neutron irradiation. Section II presents the experimental arrangements. Details about the specific image sensor are given and the description of the experiments that were carried out is shown. Section III shows the results and compares them quantitatively and qualitatively. Then, in section IV a discussion about the results that were shown is carried out and possible sources of damage are analyzed. Finally, section V presents the conclusions of the work.

II. Experimental Details

COTS CMOS sensors were irradiated with alpha particles, X-rays, and with neutrons from a neutron radiography beam, which is a mixed field of thermal neutrons and gamma rays. The aim was to compare the damage caused by those particles. The experiments were carried out using On Semiconductor CMOS monochrome image sensors model MT9M001, whose size is 0.5 inches (5:4) and it has 1280 x 1024 pixels with a pixel pitch of $5.2\,\mu\mathrm{m}$ x $5.2\,\mu\mathrm{m}$.

Figure 1 shows a cross-section of the integrated circuit taken with a Scanning Electron Microscope (SEM) and using the back-scattered electrons detector. On top of the image sensor there is a layer composed of polymers which form micro-lenses. Below this polymer, it begins the fabrication process Back End Of Line (BEOL), were metal interconnections are on top of each other, embedded and insulated by silicon dioxide. In this case the BEOL is $3.7\,\mu\mathrm{m}$ thick. Finally, the active devices, i.e. transistors and photodiodes, are located in the silicon substrate, below the Field Oxide (FOX), which is $0.3\,\mu\mathrm{m}$ thick and is composed by SiO_2 also.

Before the experiments, the glass cover was removed from the sensors allowing direct irradiation of the silicon die. Unless otherwise noted, the integration time was set to its maximum value (1033 ms) and the same was done with the gain parameter (15). Also, these sensors have an internal black level calibration function that was disabled for all the experiments in order to avoid any masking of the radiation effects. The images that were captured were recorded in video files without compression. All captures were done at room temperature. Only one sensor was exposed to ionizing radiation at a time. The particular irradiation conditions of each experiment are detailed in the next subsections.

In order to obtain the conversion factor from ADC Units (ADU) to collected charge, measured in electrons, the image sensor was exposed to Cu K_α and Fe K_α fluorescence X-rays [27]. The spectrum of collected charge was analyzed resulting in a conversion factor of $11.1\,\mathrm{e}^-/\mathrm{ADU}$ at maximum gain. Extrapolating this result for gain equal to one, a full well capacity of $42\,\mathrm{Ke}^-$ is expected.

A. Irradiation with Alpha particles

A CMOS sensor was exposed to alpha particles from an ^{241}Am source. The experiment consisted in exposing the sensor by placing the source on top of it—first taking care of removing the glass cover of the package—and then placing the whole set in a sealed box in order to isolate the sensor from ambient light.

The activity of the source was 2 kBq and it was placed at 6 mm from the sensor. The duration of experiment was 1 hour and during that time a fluence of $\simeq 1.6 \times 10^6\,\alpha\cdot\mathrm{cm}^{-2}$ was estimated.

Alpha particles from ^{241}Am source have an energy of $5.486\,\mathrm{MeV}$, but the energy of the particles arriving to the active area of the sensor is spread to lower values due to the energy loss in their path. Using the SRIM [17] code it was estimated that the energy of the particles that arrive to the silicon active area is approximately $4.15\,\mathrm{MeV}$. The distance between source and sensor and the thicknesses of the insulating layers obtained from figure 1 were taken into account for this estimation.

B. Neutron irradiation

Two CMOS sensors were also irradiated in the Neutron Imaging Facility of the RA-6 nuclear research reactor[1]. The facility beam is mainly composed by a neutron flux and residual gamma rays generated in the reactor core and passing through a Sapphire filter. The typical thermal neutron flux of the facility is $2.6 \times 10^6\,\mathrm{n(cm^2s)}^{-1}$ and the gamma dose rate 800 $\mathrm{mGy.h}^{-1}$. Although there are epithermal and fast neutrons in the neutron beam, the epithermal flux is three orders of magnitude lower than the thermal flux, in the order of $10^3\,\mathrm{n(cm^2s)}^{-1}$, and the fast flux is negligible.

The experiment consisted in the exposure of one CMOS sensor covered with a Gd_2O_3 layer of approximately $150\mu\mathrm{m}$ of thickness, and another sensor without this layer. Gadolinium has a very high absorption cross-section in the thermal neutron energy range, and acts as a blocking layer, not allowing thermal neutrons to reach the device [28]. In this way, the sensor without Gd was exposed to gamma and thermal neutrons directly from the beam, and the other sensor was exposed only to gamma rays—the thickness of the neutron

[1]RA-6 research reactor is placed in San Carlos de Bariloche city and is operated by the Argentine Atomic Energy Commission (CNEA). The purpose of this reactor is to carry out teaching, training, research and development tasks in the field of nuclear engineering. It is an extremely versatile reactor, useful for a wide range of experiments.

shielding is enough to trap most thermal neutrons but is almost transparent to gamma rays. Also, the layer can be considered as transparent to epithermal and fast neutrons, due to the low capture cross section that Gd has for energies higher than few tens of meV.

The shielding layer was prepared by making a mixture of *Microposit* S1400 photo-lithography resin and Gd_2O_3 in a powder form. The mixture was applied to the sensor over the whole die.

Both image sensors were irradiated inside the neutron radiography beam, one at a time, while recording video files from their outputs. In order to reduce the gamma dose, a lead shielding of 5 cm of thickness was placed in between the sensors and the beam. As a side effect, this lead gamma shielding reduces the thermal neutron flux so, using a neutron activation method, the neutron flux was measured at the target position resulting in $6.2 \times 10^5 \mathrm{n(cm^2 s)}^{-1} \pm 20\%$. The experiment duration was 60 minutes and during that time a thermal neutron fluence of $2.23 \times 10^9\,\mathrm{cm}^{-2} \pm \%20$ was obtained.

C. X-ray irradiation

Another sensor was exposed to radiation from an *Elekta* radiotherapy linear accelerator[2]. This equipment is capable of producing X-rays by hitting a lead target with accelerated electrons. The X-ray photons have a distribution of energy with the maximum intensity located in 2 MeV and a range from 0 to 7 MeV [29]. For the irradiation conditions, a photon flux of $2 \times 10^{10}\,(\mathrm{cm^2 s})^{-1}$ was calculated.

In order to have electronic equilibrium, the sensor was placed inside a water equivalent phantom and it was irradiated in steps of 2.7 Gy(Si) up to a total accumulated dose of 54 Gy(Si). The dose rate on each step was 60 mGy/s. During the experiment the sensor was powered and after each step a video of the dark image was recorded for 30 seconds.

III. Analysis and Results

This section presents qualitative and quantitative analysis of the damage produced by the different particles. Through the analysis of post-irradiation dark image—acquired without incident light or particles on the sensor—, the type of damage caused by each particle is compared.

Then, with the images acquired during irradiation, it is possible to detect when pixels get damaged and to correlate the damage with the particle which created it [16]. This will be used to analyze the amount of ionization produced by the particles that produce damage and also the shape and characteristic of the ionization event as seen in the captured image.

Finally, the composition of the insulating layers of the chip is studied to look into the physical mechanisms which cause the damage.

[2]This LINAC is located in San Carlos de Bariloche, Argentina, in the radiotherapy center inaugurated in January 2018, and managed by *INTECNUS*.

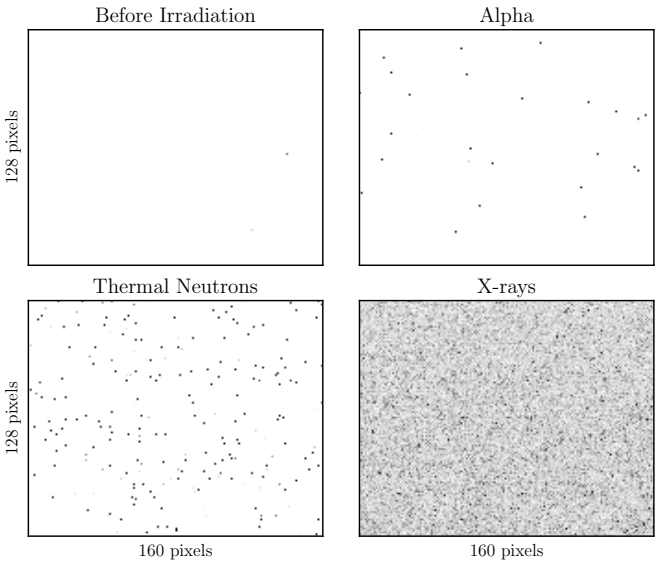

Fig. 2. Comparison of dark output images before and after irradiation. 1/8th of the original images is shown and also the color scheme was reversed for clarity, so darker colors correspond to brighter pixels. Alpha particles and thermal neutrons produce defects that are very localized, while X-ray photons increase the overall leakage. Alpha particles fluence was $1.6 \times 10^6\,\mathrm{cm}^{-2}$, thermal neutron fluence was $2.23 \times 10^9\,\mathrm{cm}^{-2}$, and X-ray photon fluence was $1.8 \times 10^{13}\,\mathrm{cm}^{-2}$ (54 Gy(Si)).

A. Dark images after irradiation

Dark images were obtained with the sensor after irradiation in order to compare the damage caused by each type of particle. Figure 2 presents the dark image of four sensors: the first not irradiated, the second irradiated with alpha particles, the third with thermal neutrons, and a fourth with X-ray photons. The image before irradiation has a few bright pixels which correspond to the typical Dark Signal Non-Uniformity (DSNU) of the sensor. However, it can be seen that when the sensor is exposed to alpha particles and thermal neutrons, a number of *hot pixels*—i.e. pixels with dark values higher than the average— appear. On the other hand, X-ray irradiation produces a smooth and uniform increase of the brightness in the whole image—and not only localized in a few pixels [16]. A result similar to that of the X-ray irradiation and for a comparable dose–51 Gy–was reported in [10] for image sensors fabricated in similar technology nodes.

B. Damage creation after particle interaction

As it was explained before, the images acquired during irradiation were recorded in video files. The data were analyzed looking at the moment in which a hot pixel is created. Figure 3 shows a typical result observed when an alpha particle released by the ^{241}Am source causes permanent damage to the sensor. The insets show three images of the region: one before the interaction, one of the exact frame in which the event took place, and finally one after the event showing the remaining *hot pixel*. The main plot shows the charge collected by each pixel around the centroid of the interaction as a function of time.

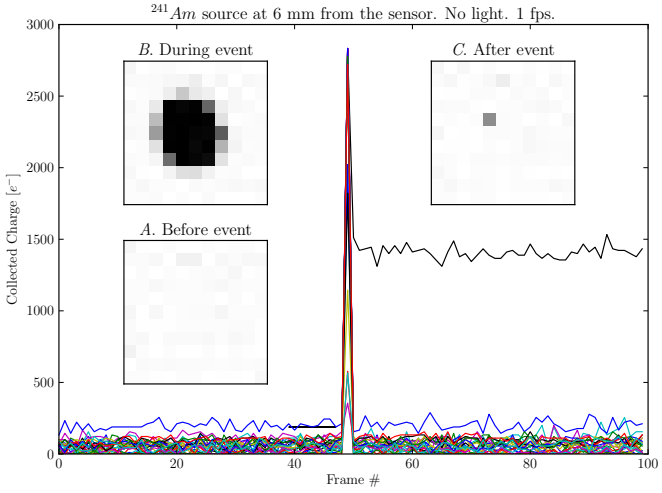

Fig. 3. Typical damage produced by alpha particles. 36 pixel values of a 6 by 6 matrix centered on the event are shown as a function of time (at 1 fps, $t_{int} = 1033\,ms$). Inset *A* shows the image before particle hit, *B* shows the frame in which the interaction took place and *C* shows the resulting image after damage.

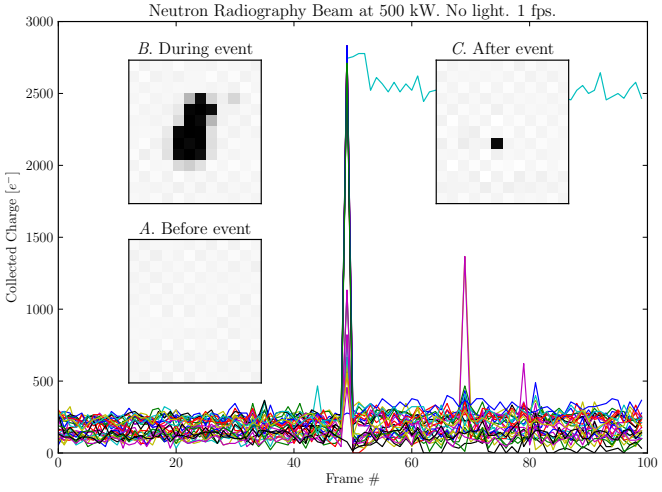

Fig. 4. Typical damage produced during the neutron radiography experiment. The values of a matrix centered on the event, are shown versus time (at 1 fps, $t_{int} = 1033\,ms$) and also the image sequence as seen in the video. Inset *A* shows the pixels before particle hit, *B* shows the frame in which interaction took place, and *C* shows the resulting damage. In frames 69 and around 80, other particles are detected without creating a permanent defect.

Before the event all pixels exhibit low baseline levels. During the event, some pixels collect ionization charge and larger values are read [9]. After the event, in the example of the figure, one pixel exhibits a permanent high base-line level, becoming a damaged *hot pixel*. This only happens in few events as will be discussed later. Actually, most of the alpha particle interactions do not cause permanent damage and the baseline level is restored to its initial value.

A similar effect was observed when the sensors are irradiated with thermal neutrons, as it is exemplified in figure 4. Again, the insets present an image before, during and after the interaction; whereas the main plot presents the values read from the pixels in a box centered on the event as a function of time. This is only an example of a typical damage which happens in a fraction of the events. It is worth noticing that in this figure, in frames 69 and around 80, other particles are detected by the sensor without creating a permanent defect.

In both figures, before the particle interaction, pixels have low baseline levels with relatively low noise. The interaction of the particle with the semiconductor produces free carriers that discharge the pixels in the neighboring area [9]. During the frame of the interaction, those pixels are shown as a very bright spot in the image because their junctions were discharged by the ionization current. The ionization current is only collected in a period of time much shorter than the frame period, and in most cases in the next frame the baseline levels of the readings are restored. However, in the few cases in which the particle produces damage, for example by the displacement of a cluster of Si atoms from their lattice position [30], the reverse biased junction current of the pixel increases leading to an increase in the baseline level. After the reset cycle, that leakage discharges the photodiodes and those pixels stay illuminated in the dark image. The leakage current continues affecting those pixels for the next frames and this is seen as a sudden change in the mean values of the pixels after the particle hit, as shown in figures 3 and 4. This behavior is typical for displacement damage in CMOS image sensors and was already reported for example for fast neutron irradiation [22], [23] and alpha particles [25], [26].

This behavior was not seen when irradiating the sensors with X-ray photons. Pixels baseline values were never suddenly modified after a single event. Only a slow and continuous increase with dose is observed uniformly in the image as was shown in Fig. 2. This suggests that the damage mechanism is different for X-rays. This increase in the dark image baseline pixel values is typical for Total Ionizing Dose (TID) effects as reported in [10].

C. Dark current increase distribution after irradiation.

In Figure 2 images obtained with the sensor before and after irradiation were shown. Now, in figure 5 a comparison of histograms of dark currents increase after the experiments is shown. Each point in the plots shows the number of pixels with a given increase in dark current. The mean dark current increases for alpha and thermal neutrons are 3.8 and $8.4\,e^-/s$ respectively, whereas the mean increase for X-rays irradiation is $613\,e^-/s$.

It can be seen that after thermal neutron irradiation the dark current of only some pixels is higher than the average, and this does not change the most probable value of the distribution. The shift after alpha irradiation is very similar and only an increase in the dark current of some pixels is seen. This result is similar to the pixel distribution reported by [22] and [23] with an exponential distribution as a result of displacement damage.

On the other hand, as was seen in the previous section, X-ray irradiation behaves differently. The dark current increase distribution is almost gaussian, which means that a large part of the pixels is shifted evenly to a higher dark current.

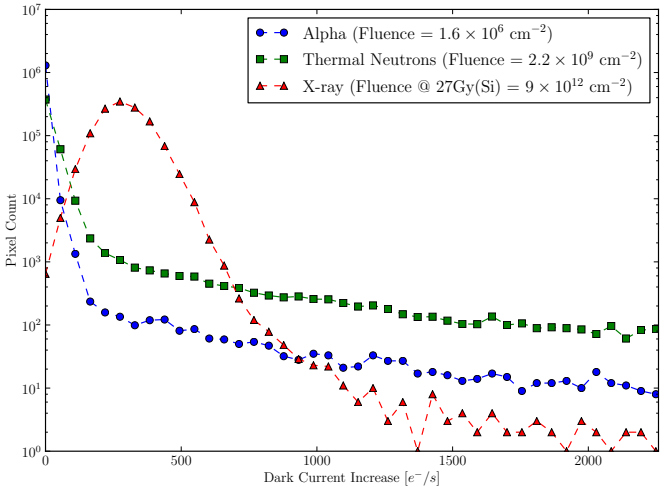

Fig. 5. Histograms showing an increase in pixel dark current after irradiation. Alpha particles and thermal neutrons present similar distributions, whereas that of X-rays irradiation is different, which is an indication that the damage mechanism is different.

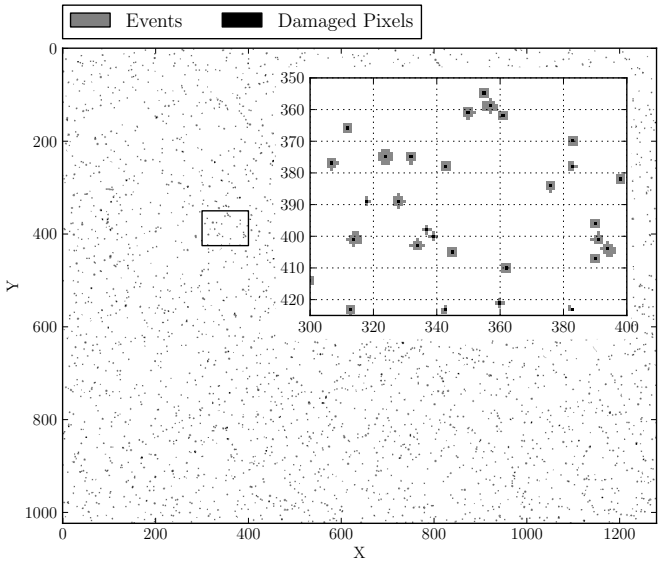

Fig. 6. Events and damaged pixels detected by processing the neutron radiography experiment video with the algorithm. A time span of 30 minutes of irradiation was analyzed and the events detected were accumulated to form the presented image. Only a fraction of the image area is shown.

Similar results were reported by [10]. This is the result of TID effects, positive charge builds-up in the dielectric layers of the integrated circuit and interface traps are created in the Si-SiO_2 interface, causing an increase in the photodiode leakage current in each pixel [31].

The histograms of Fig. 5 in turn present an alternative way to show that alpha and thermal neutrons produce very localized damage and that the leakage is concentrated in a limited number of pixels, whereas X-rays generate a more uniform damage in the whole sensor.

D. Analysis of the Damaging Events

In section III-B it was shown that through the analysis of the events in the images it is possible to detect the arrival of the particles which permanently damage pixels. In this section, an analysis of shape and intensity of the ionization events was carried out in order to see if a discrimination between particles was possible.

To do so, an event and damage detection algorithm was developed using *Python* and *OpenCV* applying a slight variation of the technique proposed in [9]. The algorithm automatically detects events produced by particle interactions looking at the difference between one frame and the next; and collects parameters of the image created by events like area, perimeter, image moments—i.e. raw and central moments—, and the sum of the intensities of all pixels involved in the event—a measurement of the ionization charge—are saved in a text file. Hot pixels creation is identified by looking for sudden changes in their mean value. When they are detected, the parameters of the event that produced the damage are saved for further processing. In this way it is possible to analyze damaging events separately from all events. The frames were analyzed using this algorithm and a statistical analysis of the events was performed.

An example of detected events and damaged pixels is shown in figure 6. There, the pixels that collected the ionization charge produced by a particle are displayed in gray, and pixels that were damaged during the same ionization event are displayed in black. All the damaged pixels created during the irradiation were correlated to its corresponding ionization event.

Alpha particles deposit a huge amount of charge in a small volume and, due to plasma effect [32], the charge is spread over several pixels producing in the image a big circular spot which can be identified. In [9], an algorithm which allows to distinguish between alpha particles and electrons or photons was presented. It is based on the fact that the amount of charge per pixel of the recorded event is proportional to the Linear Energy Transfer (LET) of the particle. So, this algorithm allows the discrimination of particles by LET.

The video taken during the thermal neutron irradiation was analyzed with this algorithm to find different patterns between all the events and the events which caused defects. Of all the events in the video, 17% were identified as particles with high LET, similar to alpha particles. When the classification criteria was applied to events which caused damage, 72% were classified as high LET particles. This suggests that the defects were created by particles which interact with Si in a similar way than alpha particles, i.e. particles with LET in the order of $0.1\,\mathrm{MeV}/\mu\mathrm{m}$ (for $4.15\,\mathrm{MeV}$ Alpha), and not by electrons or photons.

E. Sensor Composition Analysis

A Rutherford Backscattering Spectroscopy (RBS) experiment was carried out using the $1.7\,\mathrm{MV}$ tandem accelerator located at Bariloche Atomic Center [33]. The objective was to determine the presence of Boron in the image sensors. A standard setup was used, focusing on the reaction $^{11}\mathrm{B(p,}\alpha\mathrm{)Be}$. The sensors were irradiated with 2.6 MeV protons, where the reaction cross section is maximal. Alpha particles of

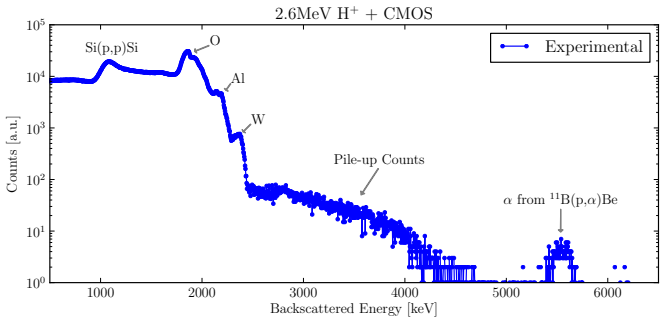

Fig. 7. Rutherford backscattering spectroscopy experimental results. The 5.6 MeV peak indicates that the sample contains Boron.

5.994 MeV are created in the reaction [34] and detected by the system. Figure 7 shows the measured back-scattered energy spectrum, which was calibrated and fitted using the SIMNRA [35] software.

The peak at 5.6 MeV is created by alpha particles released in the mentioned reaction and indicates the presence of Boron. Furthermore, the position in energy of this peak is related to the depth of the layer containing Boron. After an analysis with both SIMNRA and SRIM [36] codes, it was estimated that the layer is located at $4.3 \pm 0.5\mu$m below the surface. A fast run of the SRIM code gives a stopping power of $100\,\mathrm{keV}/\mu\mathrm{m}$ in a SiO_2 sample, which is in accordance with a loss of around $400\,\mathrm{keV}$ in the way out to the surface. This locates the Boron below the first metal layer and agrees with the standard use of BPSG as pre-metal dielectric [37], [38].

It is important to note that when the sensor was irradiated with proton energies lower than 2.6 MeV, the peak associated to alpha particles suddenly diminished, confirming the result that the peak is not caused by any other possible mechanism.

IV. Discussion

In the last section it was shown that the irradiation with the thermal neutron beam produced *hot pixels*. This section will discuss possible physical interactions with the sensor elements that could cause the increase in the photodiodes leakage current that leads to hot pixels.

As was mentioned, the neutron radiography beam comprises thermal neutrons, gamma photons, and a much smaller flux of epithermal and fast neutrons. We will discuss possible interactions between these particles and the materials used for the fabrication of the integrated circuits.

The damage observed in the sensors cannot be caused by the gamma rays for two reasons. In first place, and as was shown in the last section, the damage caused by photons is different from the damage observed in the neutron radiography beam. Gamma photons create an uniform increase in the dark current of the pixels instead of *hot pixels*. In second place, the sensor shielded against thermal neutrons with $150\mu m$ of Gd_2O_3 presented a negligible number of defects. The attenuation of this thin shielding layer for gamma rays is negligible, thus both sensors—shielded and unshielded—received the same number of photons.

The thin Gd_2O_3 layer is not sufficient to absorb fast and epithermal neutrons, because the capture cross section of Gd decreases sharply for energies higher that few meV, and the attenuation of this thin layer is insufficient to reduce the flux for these energies. Nevertheless, fast and epithermal neutrons cannot explain the damage observed in the sensor because the device shielded for thermal neutrons with Gd_2O_3 was clearly less damaged than the other.

Thus, the damage expressed as *hot pixels* should be caused by the interaction of the thermal neutrons with the devices. As it had been shown in the previous section, the insulating materials on top of the active region of the sensor comprise a thin BPSG layer which contains Boron. It is highly likely that the interaction of thermal neutrons with ^{10}B, with the release of fast alpha and ^{7}Li particles as reaction products [19], could damage the sensor. Moreover, as it was seen in section III-D, the damaging events in the neutron irradiation were similar to that of alpha particles. It is reasonable to assume that ^{7}Li ions and Alpha particles emitted from the $^{10}\mathrm{B}(\mathrm{n},\alpha)^{7}\mathrm{Li}$ nuclear reaction will leave similar patterns since both have comparable LET ($0.4\,\mathrm{MeV}/\mu\mathrm{m}$ for $0.84\,\mathrm{MeV}$ ^{7}Li ions versus $0.3\,\mathrm{MeV}/\mu\mathrm{m}$ for $1.47\,\mathrm{MeV}$ Alpha particles).

BPSG is composed generally by 2 to 8% by weight of natural Boron [19], [38], which in turn is formed by 19.9% of ^{10}B and 80.1% of ^{11}B. ^{10}B has a very high thermal neutron capture cross section, nearly a million times higher than ^{11}B, and its reaction sub-products are α and ^{7}Li particles. 94% of the times the reaction emits a gamma photon of 478 keV, an alpha particle with kinetic energy of 1.47 MeV and a ^{7}Li with 0.84 MeV. The remaining 6% of the times, the gamma photon is not emitted and the alpha and ^{7}Li are emitted with energies of 1.77 MeV and 1.01 MeV, respectively. These kinetic energies are sufficient to reach the silicon active volume from a distance of approximately 5 μm as will be shown with SRIM simulations.

Taking into account that there is a volume of 6.66 mm by 5.32 mm—image area—by 0.35 μm—thickness of (C) in figure 1—of BPSG ($\mathrm{V_{BPSG}}$), whose density is $2.22\,\mathrm{g\,cm^{-3}}$, doped with 5% of natural Boron—of which only 19.9% is ^{10}B—, the ^{10}B thermal neutron absorption cross section ($\sigma^{^{10}\mathrm{B}} = 3838$ barns [39]), and its atom density ($\mathrm{N}^{^{10}\mathrm{B}} = 1.24 \times 10^{21}\,\mathrm{cm^{-3}}$), the reaction rate was calculated for the thermal neutron irradiation experiment as:

$$\mathrm{R}_{\mathrm{n_{th}}}^{^{10}\mathrm{B}}\left(\mathrm{V_{BPSG}}\right) = \sigma^{^{10}\mathrm{B}}\,\mathrm{N}^{^{10}\mathrm{B}}\,\phi_{n_{th}}\,\mathrm{V_{BPSG}} \qquad (1)$$

Which gives 36 α and ^{7}Li released per second, so approximately 1.3×10^5 of both particles are produced in 60 minutes. Due to momentum conservation, alpha and lithium particles are emitted in opposite directions, therefore the number of particles, α or ^{7}Li, that arrive to the silicon active volume is 1.3×10^5. Dividing by the sensor area this gives a fluence of $3.7{\times}10^5\,(\alpha\,\mathrm{or}\,^{7}\mathrm{Li}).\mathrm{cm^{-2}}$. Due to the error in the measurement of the thermal neutron flux and the uncertainty in the Boron doping all these numbers have 80% of relative error.

With these results and the number of damaged pixels, a *damage factor* can be calculated as the number of damaged pixels divided by the total number of arrived particles. This

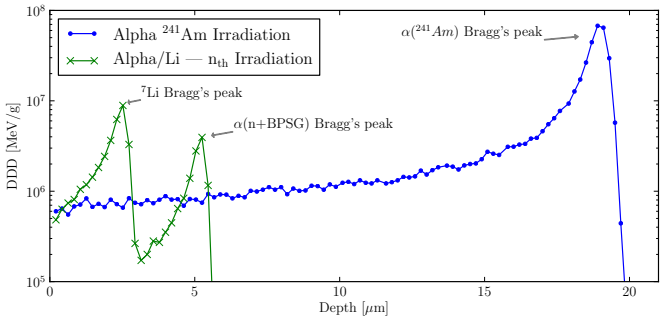

Fig. 8. Displacement damage dose (DDD) as a function of depth calculated from SRIM simulations. Zero depth is the Si-SiO_2 interface and the x-axis points towards the silicon substrate (marked in figure 1). The simulation takes into account 1.47 MeV alphas and 0.84 MeV ^{7}Li, which are the most probable particle energies after Boron neutron capture. The remaining 6% of the cases were disregarded.

gives 0.05 damaged pixels per α or ^{7}Li for the neutron radiography experiment, and 6×10^{-4} damaged pixels per alpha for the alpha experiment, where the number of arrived particles is 5.7×10^5. Thus, the particles released by neutrons produce 83 times more damage than the alpha particles of Americium.

This agrees with the displacement damage dose that was calculated from the results of SRIM [17] simulations of non-ionizing energy loss (NIEL) in Silicon using a displacement damage threshold energy of 15 eV. The procedure described in [40] was followed to obtain the NIEL as a function of particle penetration depth, and then, given the fluence in each experiment, a total displacement damage dose was calculated. Figure 8 shows the simulation results. In the alpha experiment most of the energy is deposited 19 μm below the Si-SiO_2 interface, at the position of the Bragg's peak, since those alpha particles from Americium arrive with 4.15 MeV to the Si-SiO_2 and the geometry implies that the particles have an almost normal incidence into the silicon. In the first few microns, where the silicon active volume is located—i.e. depletion regions of photodiodes—, the particles released by thermal neutrons interaction with BPSG have their Bragg's peak and so the displacement damage dose due to these particles is higher than the dose due to alpha from Americium. That could be the reason why the damage is more visible—there are more hot pixels—with less α and ^{7}Li particles.

So, alpha particles and ^{7}Li loose a part of their energy displacing Si atoms from their lattice position creating vacancies and interstitials. A single incoming particle can create a cluster of defects [30] and these defects increase the generation rate in the depletion region of reverse biased junctions explaining the increase in the dark current of the pixels.

In [41] a universal damage factor K_{dark} was proposed for silicon devices, and it has been shown that the mean dark current increase DC_{mean} is proportional to the displacement damage dose DDD and the depleted volume V_{dep} via this proportionality factor.

$$DC_{mean} = K_{dark} \times V_{dep} \times DDD \qquad (2)$$

Since the depletion volume is unknown for these devices—that is proprietary information—it is not possible to calculate a theoretical dark current increase. Nevertheless, using the information that has been gathered from the Americium experiment it is possible to calculate a depletion volume and use this volume in order to calculate the DDD for the thermal neutron experiment. Comparing this DDD calculated for the thermal neutron experiment with the expected DDD taking into account only the Alpha and Lithium particles produced by the thermal neutron capture will give an idea if this effect is displacement damage or not.

For the ^{241}Am experiment, the experimental mean dark current increase was $3.8\,e^-/s$, the DDD—calculated as the product of the NIEL of 4.15 MeV Alpha particles by the fluence—was 2 TeV/g and K_{dark} equals to $0.13\,e^-/\mu m^3/s/(TeV/g)$. This K_{dark} is corrected by temperature using an activation energy of 0.63 eV for 18 degrees Celcius and, by applying an scaling factor of 1.5, it is also corrected for an annealing time of 15 hours. Solving for the depletion volume in equation 2 we obtain $14\,\mu m^3$, which is reasonable for the $5.2\,\mu m \times 5.2\,\mu m$ pixel size. The K_{dark} and fluence relative errors add a dispersion of $\pm50\%$ to the depleted volume.

For the thermal neutrons experiment, the mean dark current increase was $8.4\,e^-/s$ and K_{dark} equals to $0.221\,e^-/\mu m^3/s/(TeV/g)$—corrected for a temperature of 20 degrees Celcius and, by applying an scaling factor of 2.08, for an annealing time of 30 minutes—, knowing the depletion volume, the DDD can be calculated from equation 2 and it gives 3 TeV/g. Taking into account the relative uncertainty of each parameter, this number has an error of $\pm80\%$.

Using the α and ^7Li fluence that was calculated above with equation 1 ($\Phi = 3.7\times10^5$ (α or ^{7}Li).cm^{-2}), and the NIEL of each particle, the expected DDD is calculated as:

$$DDD_{expec} = (NIEL_\alpha + NIEL_{^7Li}) \times \Phi/2 \qquad (3)$$

Which gives $1.6\,TeV/g \pm 20\%$ for the thermal neutrons experiments. Taking into account all the uncertainties, this DDD predicted from the thermal neutron fluence is in close agreement to the DDD estimated from the increase in the dark current observed in the sensors. This result supports the hypothesis that states that Boron thermal neutron capture is the responsible for the damage seen in the devices.

At this point it is possible to estimate the total ionizing dose deposited into the sensor in order to compare the X-ray with Alpha and thermal neutron irradiations. The total ionizing dose can be estimated by multiplying the LET of the particle by the fluence, which gives a TID of 0.1 Gy(Si) for the ^{241}Am experiment (Alpha LET $= 431\,MeV.cm^2/g$). In the thermal neutron experiment the ionizing particles are the Alpha (LET $= 1148\,MeV.cm^2/g$) and ^{7}Li ions (LET $= 1724\,MeV.cm^2/g$) produced by the Boron thermal neutron capture, and the fluence depends on the Boron doping of BPSG and was calculated in equation 1. So, the TID for the thermal neutron experiment was approximately 0.08 Gy(Si). Hence, both total ionizing doses are negligible when compared to the 27 Gy(Si) of the X-ray experiment and for that reason there is no shift to the right in the distribution of Alpha and thermal neutron dark current increase histograms of figure 5.

Other interactions of thermal neutrons with materials

present in the sensor are discarded. Sensor composition is mainly natural Silicon, i.e. ^{28}Si 92.2%, ^{29}Si 4.7% and ^{30}Si 3.1%. Thermal neutrons interaction mechanism is by nuclear absorption. Consequently, when a neutron is captured by ^{28}Si, stable ^{29}Si will be produced, which does not disrupt the silicon lattice. The same happens with ^{29}Si, it becomes ^{30}Si which is also stable. Conversely, when a thermal neutron is captured by ^{30}Si, the produced ^{31}Si is unstable and decays in ^{31}P within a couple of hours by beta emission. ^{31}P has one extra electron which becomes a free carrier in the silicon lattice and thus this is the same as a doping process with donor atoms. The addition of minority carriers in a P-type silicon substrate increases the reverse bias leakage current of photodiodes and may lead to the generation of hot pixels.

In order to see if this doping by silicon transmutation was relevant, the reaction rate in the neutron radiography experiment was calculated as

$$\mathrm{R}_{\mathrm{n_{th}}}^{^{30}\mathrm{Si}} = \sigma^{^{30}\mathrm{Si}}\, \mathrm{N}^{^{30}\mathrm{Si}}\, \phi_{n_{th}} \tag{4}$$

where $\sigma^{^{30}\mathrm{Si}}$ is the microscopic thermal neutron absorption cross section of ^{30}Si ($0.107\,\mathrm{barns}$ [39]), $\mathrm{N}^{^{30}\mathrm{Si}}$ is its atom density, and ϕ_n is the thermal neutron flux ($6.2 \times 10^5 \mathrm{n(cm^2 s)^{-1}} \pm 20\%$). This gives the reaction rate in reactions per unit of volume and time. Taking into account a duration of the experiment of 60 minutes, the number of silicon atoms per cm^3 that decayed into phosphorous is:

$$\mathrm{R}_{\mathrm{n_{th}}}^{^{30}\mathrm{Si}}\,(60\mathrm{min}) = 3.6 \times 10^5\,\mathrm{at.\,cm^{-3}} \pm 20\% \tag{5}$$

Comparing this number to a normal silicon substrate doping higher than $10^{16}\,\mathrm{at.\,cm^{-3}}$ makes it completely irrelevant. Therefore this can not be the reason of the leakage increase.

Finally, other isotopes that could capture thermal neutrons, like ^{16}O, have very low thermal neutron capture cross sections or are present in very small amounts like metals used for interconnections. So they are not a relevant source of particles that can cause damage to the silicon active region.

V. Conclusions

The irradiation of CMOS image sensors in a mixed field with thermal neutrons and gamma photons leads to the creation of *hot pixels*. To investigate into the physical mechanisms which create the damage, image sensors were irradiated with alpha particles and X-ray photons.

The different characteristics of the observed defects and the fact that a sensor shielded with a Gd_2O_3 layer did not exhibit damage, show that the effect observed is caused by thermal neutrons and not by other particles present in the neutron irradiation beam.

The interaction of thermal neutrons with ^{10}B present in a BPSG layer was proposed as a possible cause of the defect creation. To investigate this possibility, a Rutherford Backscattering Spectroscopy technique was used to confirm that the devices contain Boron. The concentrations of B usually found in the BPSG layer and the fact that the range of the particles released after Boron neutron capture is less than the Americium alpha range, can explain why the number of defects observed in the neutron experiment is greater than that of the Americium experiment. This is despite the fact that the fluence of alpha and ^{7}Li particles is less in the thermal neutron experiment than the fluence of alpha particles in the Americium experiment. The proposed mechanism for the displacement damage of the sensors is that thermal neutrons are captured in ^{10}B with the release of an alpha particle and a fast ^{7}Li ion.

The results presented in this work have implications if a CMOS sensor is intended to be used as a thermal neutron detector covered with a conversion material, since the sensor will suffer from aging as the sensor is used.

Acknowledgments

The authors would like to thank to Julio Marín, Juan Loghino and the staff of the RA-6 Nuclear Research Reactor for their assistance during the experiments; the Instituto Nacional de Tecnología Industrial for the use of the Focus Ion Beam; Simón Claramonte for his help with the sample preparation and polishing; Paula Troyon from the Materials Characterization Department of CNEA for her advice and assistance with the SEM operation; and finally the authors would like to thank to Julieta Irazoqui and Dario Sanz from INTECNUS for her assistance with the operation of the LINAC and his support to this line of investigation, respectively.

References

[1] Y. Degerli, F. Guilloux, and F. Orsini, "A novel CMOS sensor with in-pixel auto-zeroed discrimination for charged particle tracking," *Journal of Instrumentation*, vol. 9, no. 05, p. C05018, 2014.

[2] M. Paolucci, D. Battisti, M. Biasini, B. Checcucci, R. Di Lorenzo, A. Esposito, L. Fanò, D. Passeri, P. Placidi, and L. Servoli, "A real time active pixel dosimeter for interventional radiology," *Radiation Measurements*, vol. 46, no. 11, pp. 1271–1276, 2011.

[3] I. Perić, C. Kreidl, and P. Fischer, "Particle pixel detectors in high-voltage CMOS technology—new achievements," *Nuclear Instruments and Methods in Physics Research Section A: Accelerators, Spectrometers, Detectors and Associated Equipment*, vol. 650, no. 1, pp. 158–162, 2011.

[4] R. Turchetta, J. Berst, B. Casadei, G. Claus, C. Colledani, W. Dulinski, Y. Hu, D. Husson, J. Le Normand, J. Riester *et al.*, "A monolithic active pixel sensor for charged particle tracking and imaging using standard VLSI CMOS technology," *Nuclear Instruments and Methods in Physics Research Section A: Accelerators, Spectrometers, Detectors and Associated Equipment*, vol. 458, no. 3, pp. 677–689, 2001.

[5] M. Vanstalle, D. Husson, S. Higueret, M. Trocmé, T. Lê, and A. Nourreddine, "Demonstrating the γ-transparency of a CMOS pixel detector for a future neutron dosimeter," *Nuclear Instruments and Methods in Physics Research Section A: Accelerators, Spectrometers, Detectors and Associated Equipment*, vol. 662, no. 1, pp. 45–48, 2012.

[6] E. Conti, P. Placidi, M. Biasini, L. Bissi, A. Calandra, B. Checcucci, S. Chiocchini, R. Cicioni, R. Di Lorenzo, A. C. Dipilato *et al.*, "Use of a CMOS image sensor for an active personal dosimeter in interventional radiology," *Instrumentation and Measurement, IEEE Transactions on*, vol. 62, no. 5, pp. 1065–1072, 2013.

[7] S. Meroli, D. Biagetti, D. Passeri, P. Placidi, L. Servoli, and P. Tucceri, "A grazing angle technique to measure the charge collection efficiency for CMOS active pixel sensors," *Nuclear Instruments and Methods in Physics Research Section A: Accelerators, Spectrometers, Detectors and Associated Equipment*, vol. 650, no. 1, pp. 230–234, 2011.

[8] M. Perez, M. S. Haro, I. Sidelnik, L. Tozzi, D. R. Brito, C. Mora, J. J. Blostein, M. G. Berisso, and J. Lipovetzky, "Commercial CMOS pixel array for beta and gamma radiation particle counting," in *Micro-Nanoelectronics, Technology and Applications (EAMTA), 2015 Argentine School of*, July 2015, pp. 11–16.

[9] M. Pérez, J. Lipovetzky, M. S. Haro, I. Sidelnik, J. J. Blostein, F. A. Bessia, and M. G. Berisso, "Particle detection and classification using commercial off the shelf CMOS image sensors," *Nuclear Instruments and Methods in Physics Research Section A: Accelerators, Spectrometers, Detectors and Associated Equipment*, vol. 827, pp. 171 – 180, 2016. [Online]. Available: http://www.sciencedirect.com/science/article/pii/S0168900216302844

[10] X. Shoulong, Z. Shuliang, and H. Youjun, "γ-ray detection using commercial off-the-shelf CMOS and CCD image sensors," *IEEE Sensors Journal*, vol. 17, no. 20, pp. 6599–6604, Oct 2017.

[11] J. Jerónimo Blostein, J. Estrada, A. Tartaglione, M. Sofo Haro, G. Fernández Moroni, and G. Cancelo, "Development of a novel neutron detection technique by using a boron layer coating a Charge Coupled Device," *Journal of Instrumentation 10 P01006*, 2015. [Online]. Available: http://dx.doi.org/10.1088/1748-0221/10/01/P01006

[12] Y. Zhang, C. Hu-Guo, D. Husson, S. Higueret, T.-D. Lê, and Y. Hu, "Design of a monolithic CMOS sensor for high efficiency neutron counting," *Microelectronics Journal*, vol. 43, no. 11, pp. 730–736, 2012.

[13] C. Guardiola, C. Fleta, G. Pellegrini, F. García, D. Quirion, J. Rodríguez, and M. Lozano, "Ultra-thin 3d silicon sensors for neutron detection," *Journal of Instrumentation*, vol. 7, no. 03, p. P03006, 2012.

[14] M. Pérez, J. J. Blostein, F. A. Bessia, A. Tartaglione, I. Sidelnik, M. S. Haro, S. Suárez, M. L. Gimenez, M. G. Berisso, and J. Lipovetzky, "Thermal neutron detector based on COTS CMOS imagers and a conversion layer containing Gadolinium," *Nuclear Instruments and Methods in Physics Research Section A: Accelerators, Spectrometers, Detectors and Associated Equipment*, vol. 893, pp. 157 – 163, 2018. [Online]. Available: http://www.sciencedirect.com/science/article/pii/S0168900218303681

[15] Tartaglione A., Lipovetzky J., Gomez Berisso M., Pérez M., Alcalde Bessia F., Sidelnik I., Sofo Haro M., Blostein J.J., Pastoriza H., "Detector de neutrones térmicos y subtérmicos de alta resolución espacial en dos dimensiones basado en sensores electrónicos CCD y CMOS y un conversor que contiene gadolinio," June 2016, INPI patent presentation number 2016011772.

[16] F. A. Bessia, M. Perez, I. Sidelnik, M. S. Haro, J. J. Blostein, M. G. Berisso, J. Marin, and J. Lipovetzky, "COTS CMOS active pixel sensors damage after alpha, thermal neutron, and gamma irradiation," in *2016 Argentine Conference of Micro-Nanoelectronics, Technology and Applications (CAMTA)*, Aug 2016, pp. 22–26.

[17] J. F. Ziegler, M. Ziegler, and J. Biersack, "SRIM – the stopping and range of ions in matter (2010)," *Nuclear Instruments and Methods in Physics Research Section B: Beam Interactions with Materials and Atoms*, vol. 268, no. 11, pp. 1818 – 1823, 2010, 19th International Conference on Ion Beam Analysis. [Online]. Available: http://www.sciencedirect.com/science/article/pii/S0168583X10001862

[18] R. Baumann, T. Hossain, E. Smith, S. Murata, and H. Kitagawa, "Boron as a primary source of radiation in high density drams," in *1995 Symposium on VLSI Technology. Digest of Technical Papers*, June 1995, pp. 81–82.

[19] R. Baumann, T. Hossain, S. Murata, and H. Kitagawa, "Boron compounds as a dominant source of alpha particles in semiconductor devices," in *Reliability Physics Symposium, 1995. 33rd Annual Proceedings., IEEE International*, April 1995, pp. 297–302.

[20] T. Hossain, D. Posey, C. Fullwood, and M. Clopton, "Neutron intercepting silicon chip (NISC) - a sensitive neutron detector," in *2007 IEEE Nuclear Science Symposium Conference Record*, vol. 2, Oct 2007, pp. 1498–1499.

[21] K. Unlu, C. Celik, V. Narayanan, and T. Z. Hossain, "Investigation of critical charge and sensitive volume of the neutron intercepting silicon chip (NISC)," in *2013 3rd International Conference on Advancements in Nuclear Instrumentation, Measurement Methods and their Applications (ANIMMA)*, June 2013. DOI: 10.1109/ANIMMA.2013.6727921, pp. 1088–1093.

[22] A. J. P. Theuwissen, "Influence of terrestrial cosmic rays on the reliability of CCD image sensors;part 1: Experiments at room temperature," *IEEE Transactions on Electron Devices*, vol. 54, no. 12, pp. 3260–3266, Dec 2007.

[23] ——, "Influence of terrestrial cosmic rays on the reliability of CCD image sensors;part 2: Experiments at elevated temperature," *IEEE Transactions on Electron Devices*, vol. 55, no. 9, pp. 2324–2328, Sept 2008.

[24] G. H. Chapman, R. Thomas, R. Thomas, I. Koren, and Z. Koren, "Experimental study and analysis of soft and permanent errors in digital cameras," in *2016 IEEE International Symposium on Defect and Fault Tolerance in VLSI and Nanotechnology Systems (DFT)*, Sept 2016, pp. 11–14.

[25] J. M. Belloir, V. Goiffon, C. Virmontois, M. Raine, P. Paillet, P. Magnan, and O. Gilard, "Dark current spectroscopy on alpha irradiated CMOS image sensors," in *2015 15th European Conference on Radiation and Its Effects on Components and Systems (RADECS)*, Sept 2015. DOI: 10.1109/RADECS.2015.7365597, pp. 215–218.

[26] J.-M. Belloir, V. Goiffon, C. Virmontois, P. Paillet, M. Raine, P. Magnan, and O. Gilard, "Dark current spectroscopy on alpha irradiated pinned photodiode CMOS image sensors," *IEEE Transactions on Nuclear Science*, vol. 63, no. 4, pp. 2183–2192, 2016.

[27] D. W. Lane, "X-ray imaging and spectroscopy using low cost COTS CMOS sensors," *Nuclear Instruments and Methods in Physics Research Section B: Beam Interactions with Materials and Atoms*, vol. 284, pp. 29 – 32, 2012, e-MRS 2011 Spring Meeting, Symposium M: X-ray techniques for materials research-from laboratory sources to free electron lasers. [Online]. Available: http://www.sciencedirect.com/science/article/pii/S0168583X11008408

[28] D. A. Abdushukurov, M. A. Abduvokhidov, D. V. Bondarenko, K. K. Muminov, T. A. Toshov, and D. Y. Chistyakov, "Modeling the registration efficiency of thermal neutrons by gadolinium foils," *Journal of Instrumentation*, vol. 2, no. 04, p. P04001, 2007. [Online]. Available: http://stacks.iop.org/1748-0221/2/i=04/a=P04001

[29] M. Fippel, F. Haryanto, O. Dohm, F. Nüsslin, and S. Kriesen, "A virtual photon energy fluence model for monte carlo dose calculation," *Medical Physics*, vol. 30, no. 3, pp. 301–311, 2003.

[30] J. Srour, C. J. Marshall, and P. W. Marshall, "Review of displacement damage effects in silicon devices," *IEEE Transactions on Nuclear Science*, vol. 50, no. 3, pp. 653–670, 2003.

[31] V. Goiffon, "Ch.11 - Radiation Effects on CMOS Active Pixel Image Sensors," in *Ionizing Radiation Effects in Electronics From Memories to Imagers.* CRC Press, 2015.

[32] J. Estrada, J. Molina, J. Blostein, and G. Fernandez, "Plasma effect in silicon charge coupled devices (CCDs)," *Nuclear Instruments and Methods in Physics Research Section A: Accelerators, Spectrometers, Detectors and Associated Equipment*, vol. 665, pp. 90–93, 2011.

[33] S. Limandri, C. Olivares, L. Rodriguez, G. Bernardi, and S. Suárez, "PIXE facility at Centro Atómico Bariloche," *Nuclear Instruments and Methods in Physics Research Section B: Beam Interactions with Materials and Atoms*, vol. 318, no. Part A, pp. 47 – 50, 2014, the 13th International Conference on Particle Induced X-ray Emission (PIXE 2013). [Online]. Available: http://www.sciencedirect.com/science/article/pii/S0168583X13007751

[34] M. Mayer, A. Annen, W. Jacob, and S. Grigull, "The 11B(p,a)8Be nuclear reaction and 11B(p,p)11B backscattering cross sections for analytical purposes," *Nuclear Instruments and Methods in Physics Research Section B: Beam Interactions with Materials and Atoms*, vol. 143, no. 3, pp. 244 – 252, 1998, data retrieved from the IBANDL database, IAEA, 2018 at http://www-nds.iaea.org/ibandl/. [Online]. Available: http://www.sciencedirect.com/science/article/pii/S0168583X98003838

[35] M. Mayer, "SIMNRA: Computer simulation of RBS, ERDA and NRA (with license number in name of Sergio Suárez)," http://home.mpcdf.mpg.de/~mam/index.html.

[36] J. F. Ziegler, M. D. Ziegler, and J. P. Biersack, "SRIM–the stopping and range of ions in matter (2010)," *Nuclear Instruments and Methods in Physics Research Section B: Beam Interactions with Materials and Atoms*, vol. 268, no. 11, pp. 1818–1823, 2010.

[37] V. Vasilyev, C.-C. Lin, F. Gn, and A. Cuthbertson, "Comparative analysis of pre-metal dielectric gap-fill capability for ULSI device applications," vol. 8, 01 1999.

[38] M. Kirchhoff, M. Ilg, and D. Cote, "Application of borophosphosilicate glass (BPSG) in microelectronic processing," *Berichte der Bunsengesellschaft für physikalische Chemie*, vol. 100, no. 9, pp. 1434–1437. [Online]. Available: https://onlinelibrary.wiley.com/doi/abs/10.1002/bbpc.19961000914

[39] S. F. Mughabghab, *Atlas of Neutron Resonances: Resonance Parameters and Thermal Cross Sections. Z= 1-100*. Elsevier, 2006.

[40] S. Messenger, E. Burke, G. Summers, M. Xapsos, R. Walters, E. Jackson, and B. Weaver, "Nonionizing energy loss (NIEL) for heavy ions," *IEEE Transactions on Nuclear Science*, vol. 46, no. 6, pp. 1595–1602, 1999.

[41] J. R. Srour and D. H. Lo, "Universal damage factor for radiation-induced dark current in silicon devices," *IEEE Transactions on Nuclear Science*, vol. 47, no. 6, pp. 2451–2459, Dec 2000.